Supplement 1: Spatial extent of recent laboratory studies

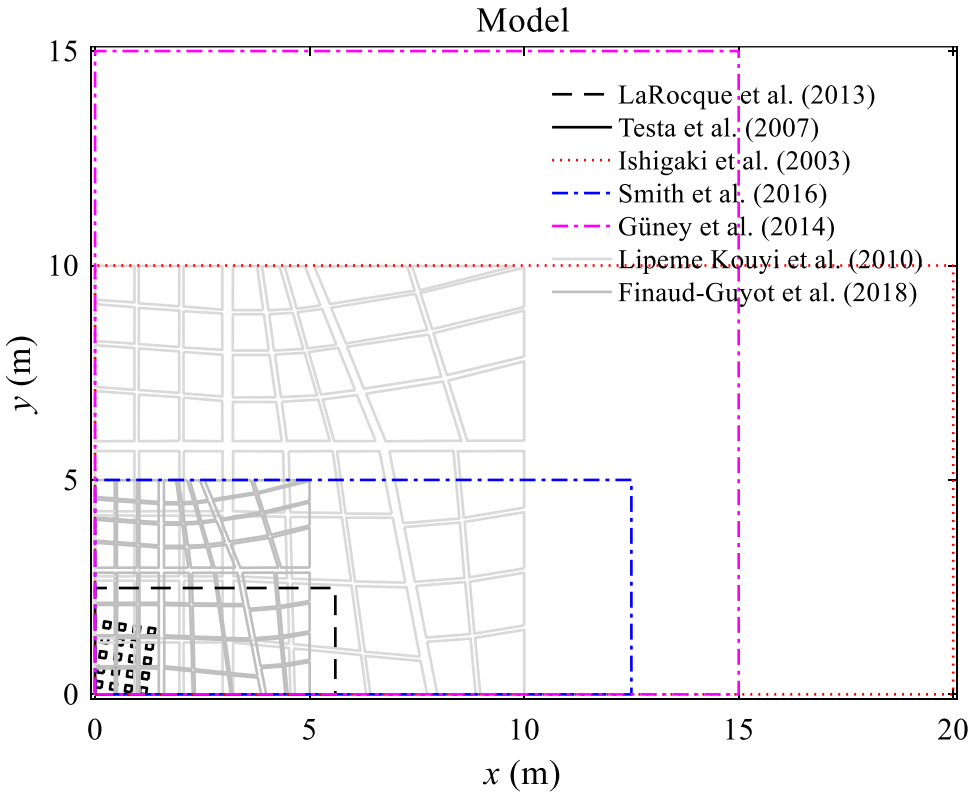

Figure S1: Spatial extent of some recent laboratory models of urban flooding

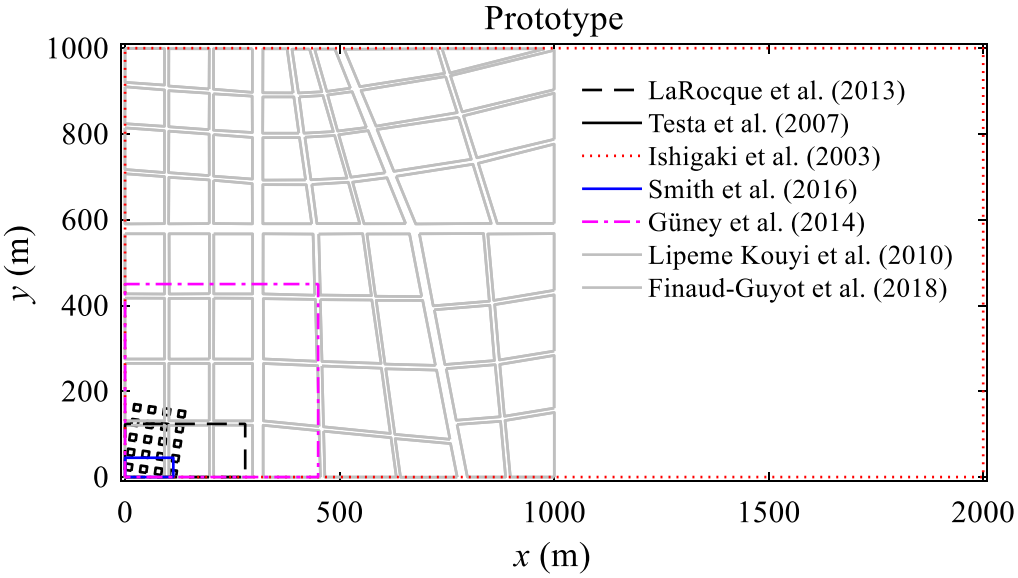

Figure S2: Spatial extent of the real-world urban area represented in recent laboratory models of urban flooding (the spatial extent for Lipeme Kouyi et al. (2010) and Finaud-Guyot et al. (2018) are the same)

Supplement 2: Location of water depths measurements in the dataset presented by Araud (2012) and Velickovic et al. (2017)

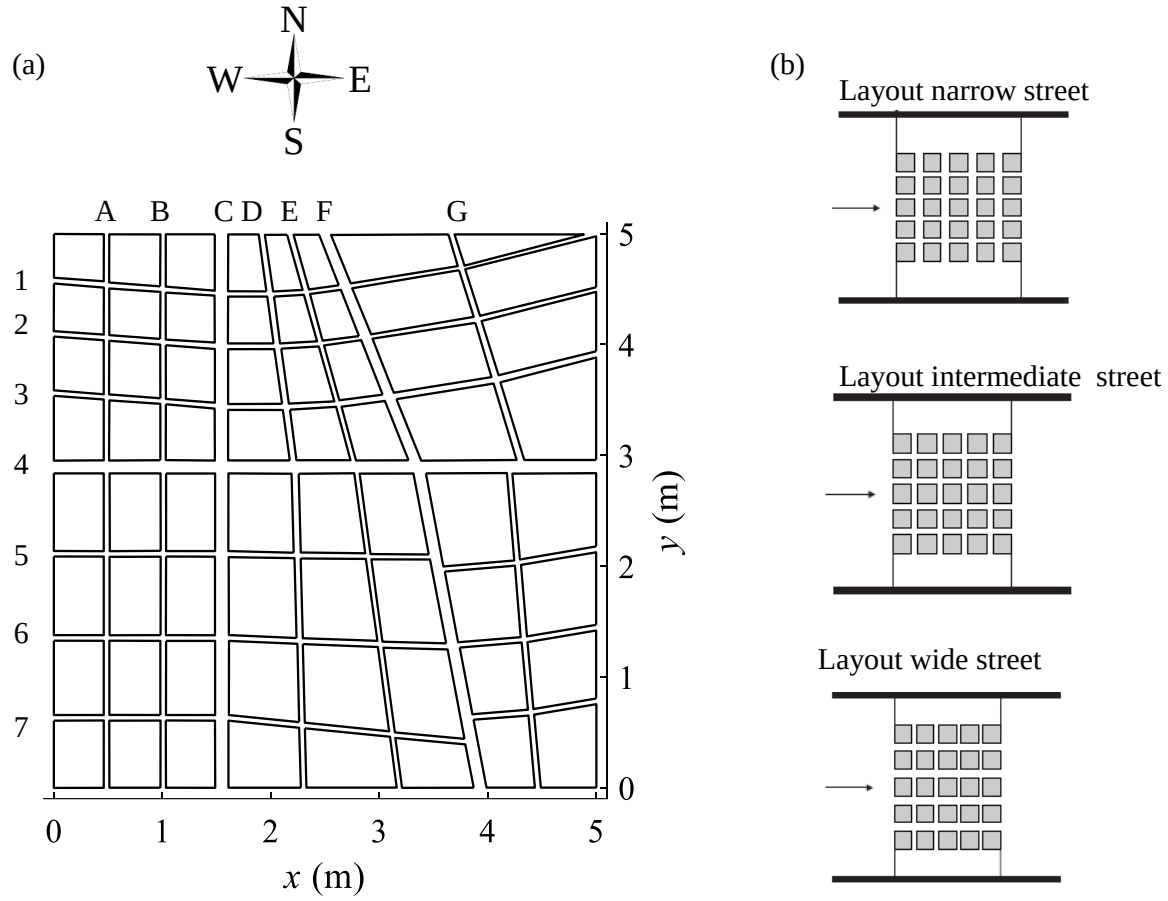

Figure S3 : Experimental plan of (a) Araud (2012), and (b) Velickovic et al. (2017)

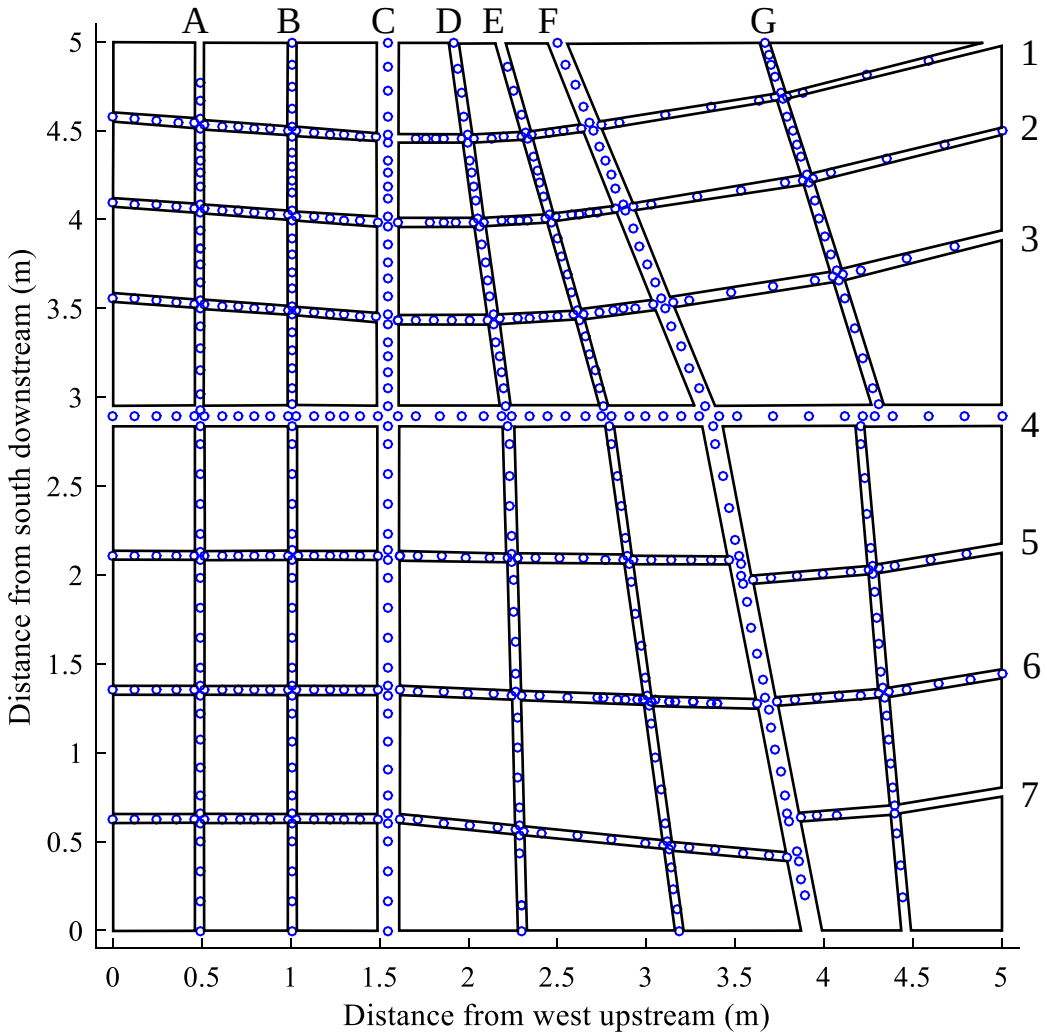

Figure S4: Location of water depth measurements in the experimental run by Araud (2012) with an inflow discharge of 20 m^3h^{-1}

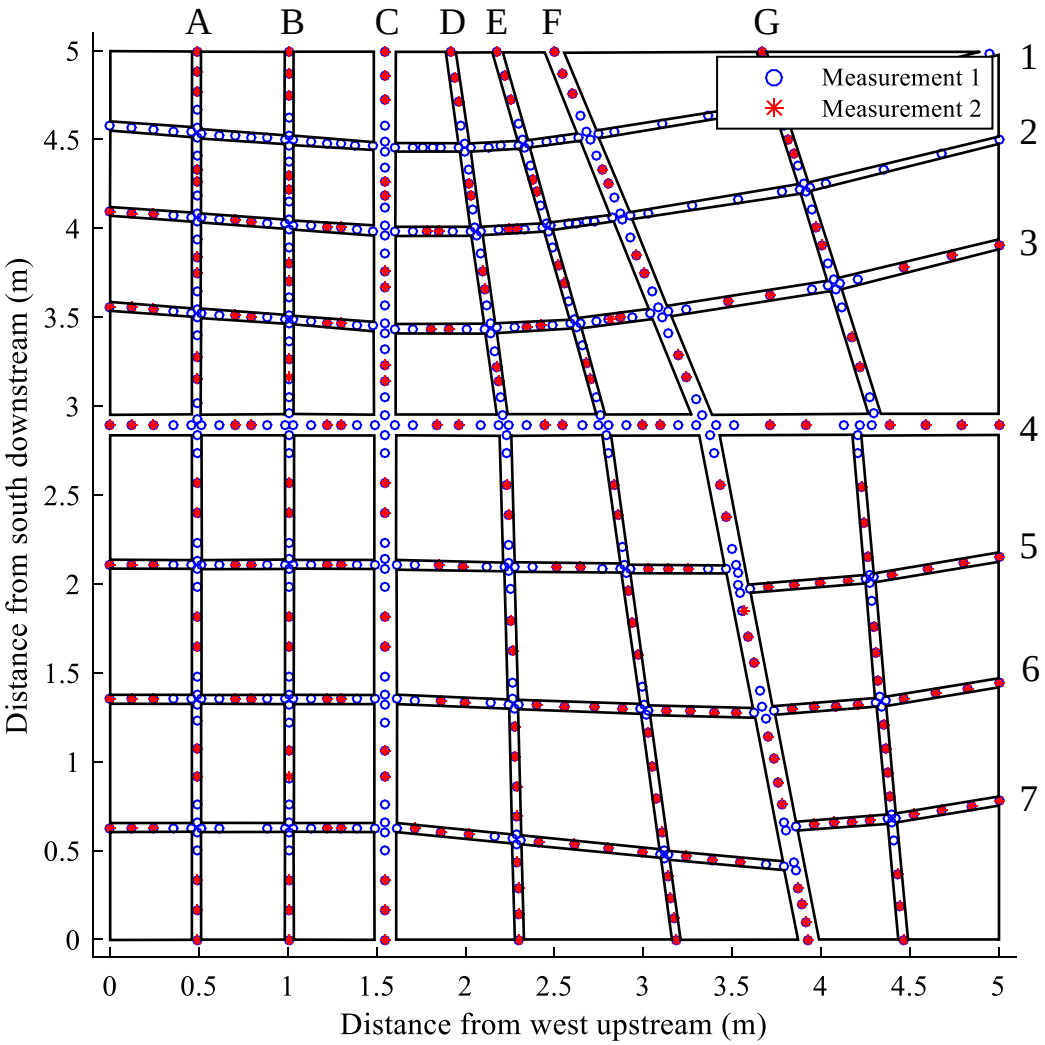

Figure S5: Location of water depth measurements (with repetition) in the experimental run by Araud (2012) with an inflow discharge of 60 m^3h^{-1}

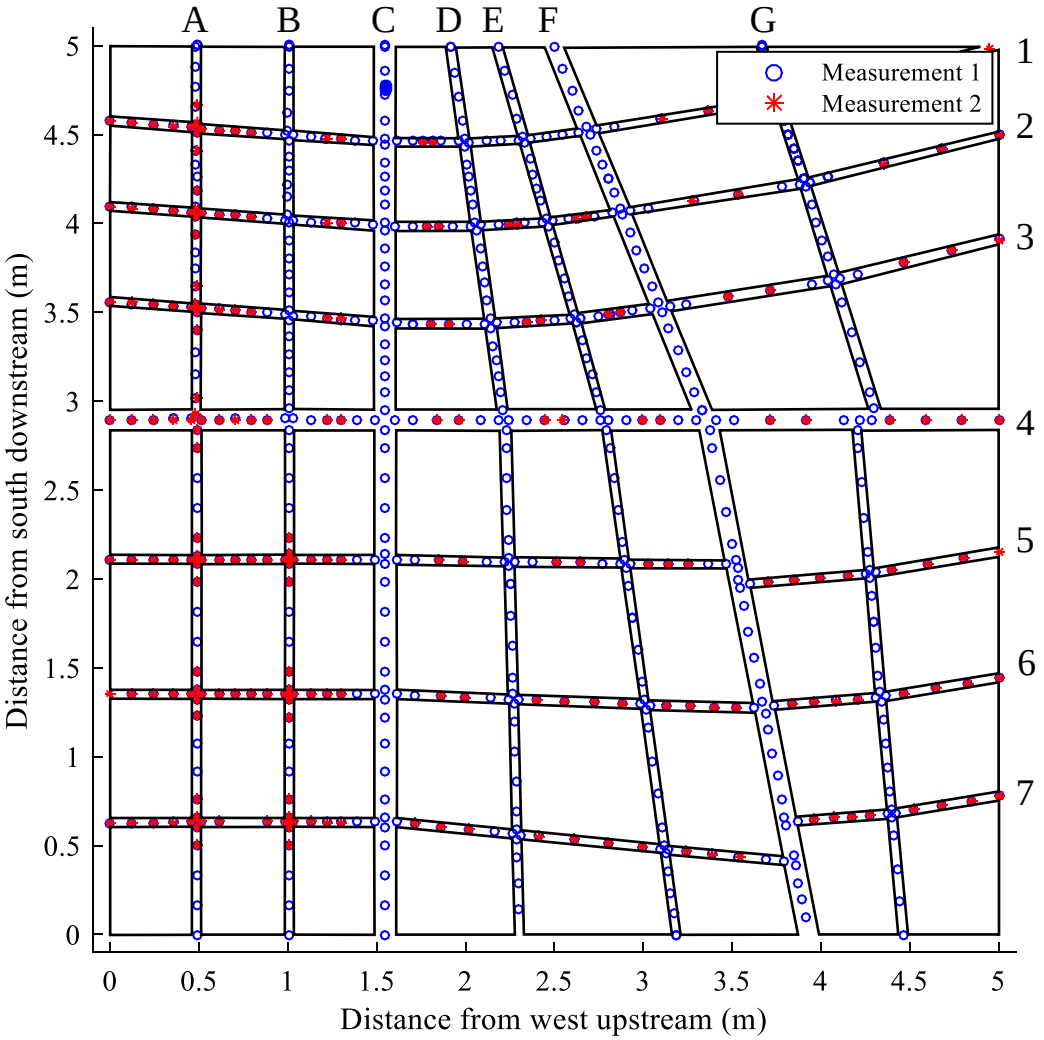

Figure S6: Location of water depth measurements (with repetition) in the experimental run by Araud (2012) with an inflow discharge of 80 m^3h^{-1}

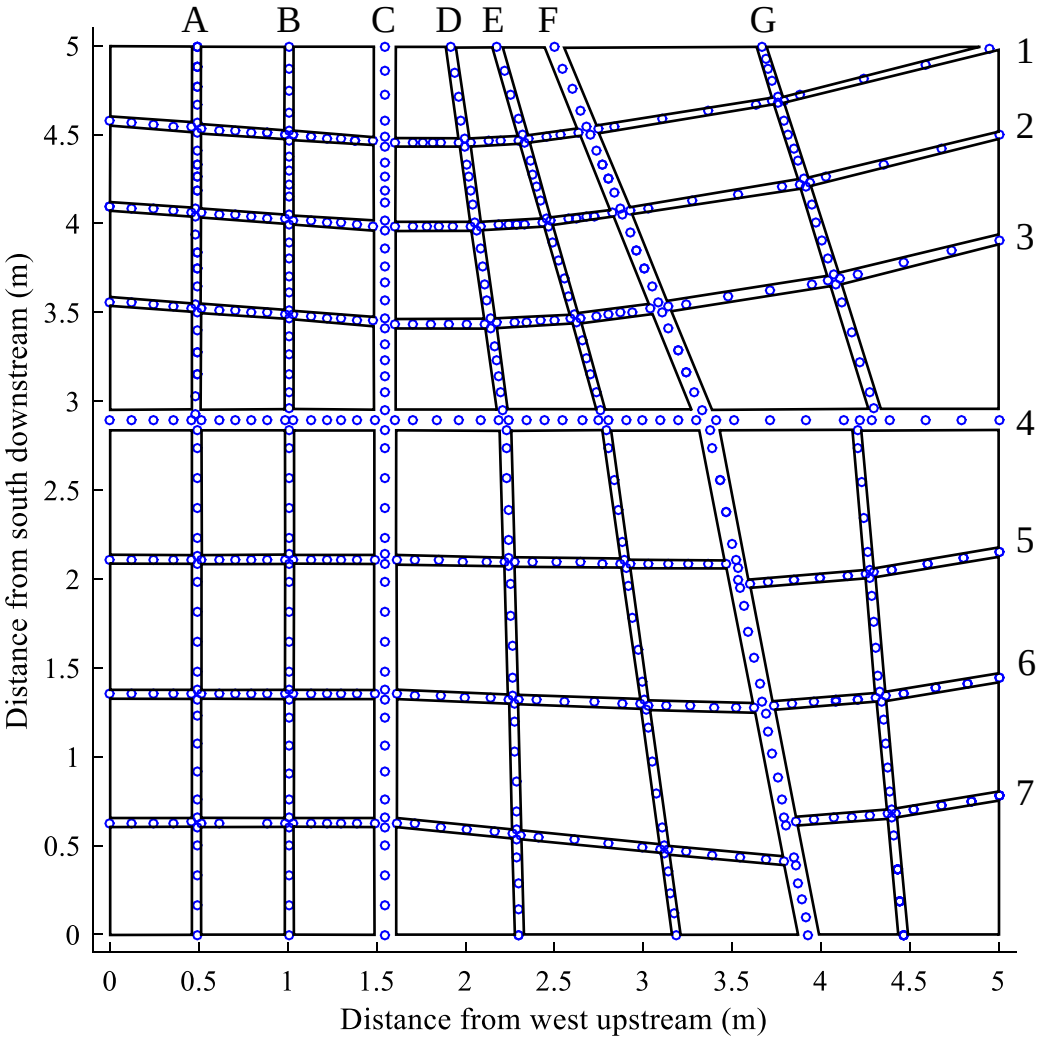

Figure S7: Location of water depth measurements in the experimental run by Araud (2012) with an inflow discharge of 100 m^3h^{-1}

Supplement 3: Variations in measured water depths between test repetitions

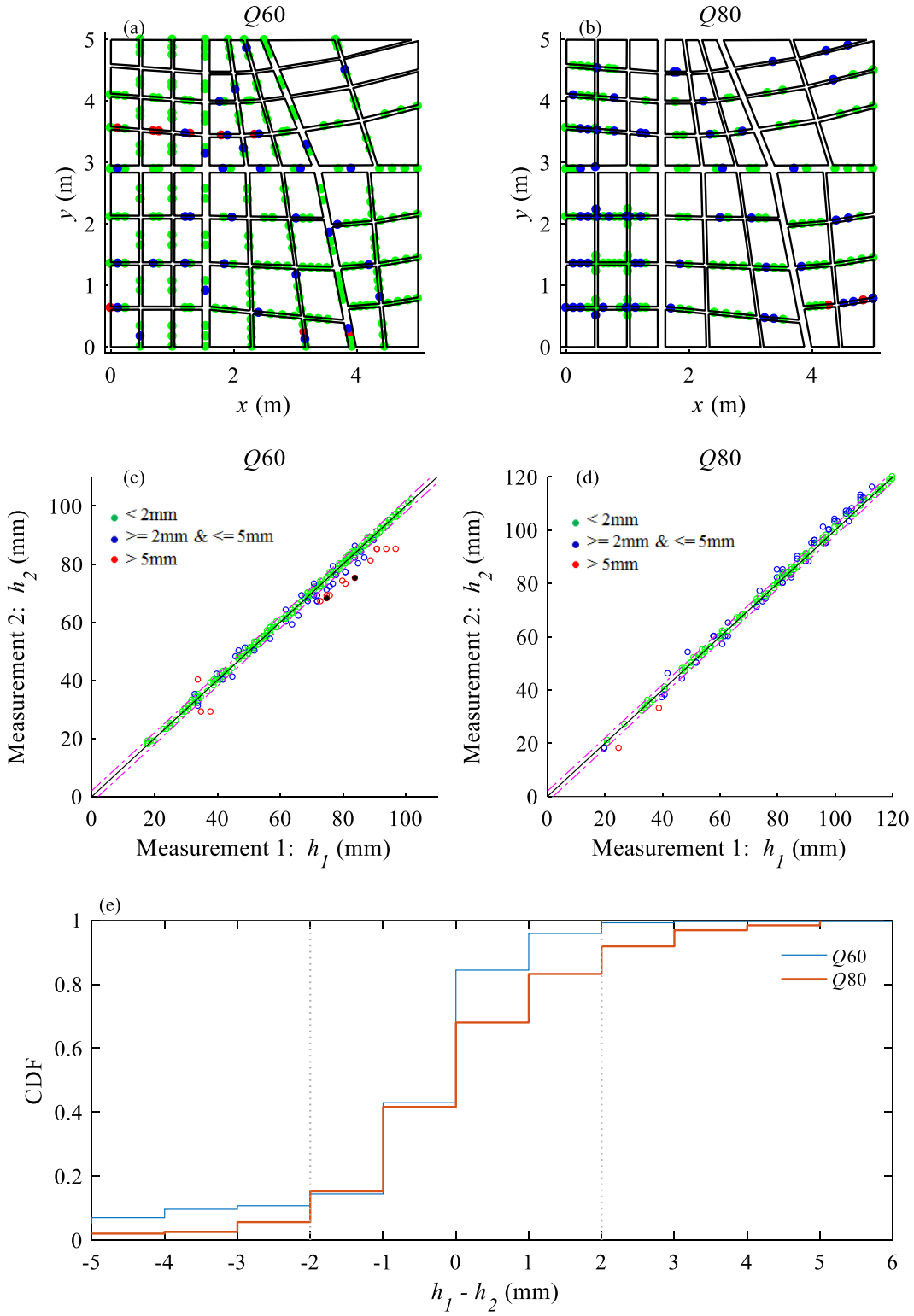

Figure S8: Analysis of the reproducibility of Run 3 (60 m^3h^{-1}) and Run 2 (80 m^3h^{-1}) presented by Araud (2012): (a) and (b) spatial distribution of the differences in measured water depth; (c) and (d) scatter plot of the water depths recorded in the two series of measurements; (e) and cumulative distribution function (CDF) of the difference in measured water depths.

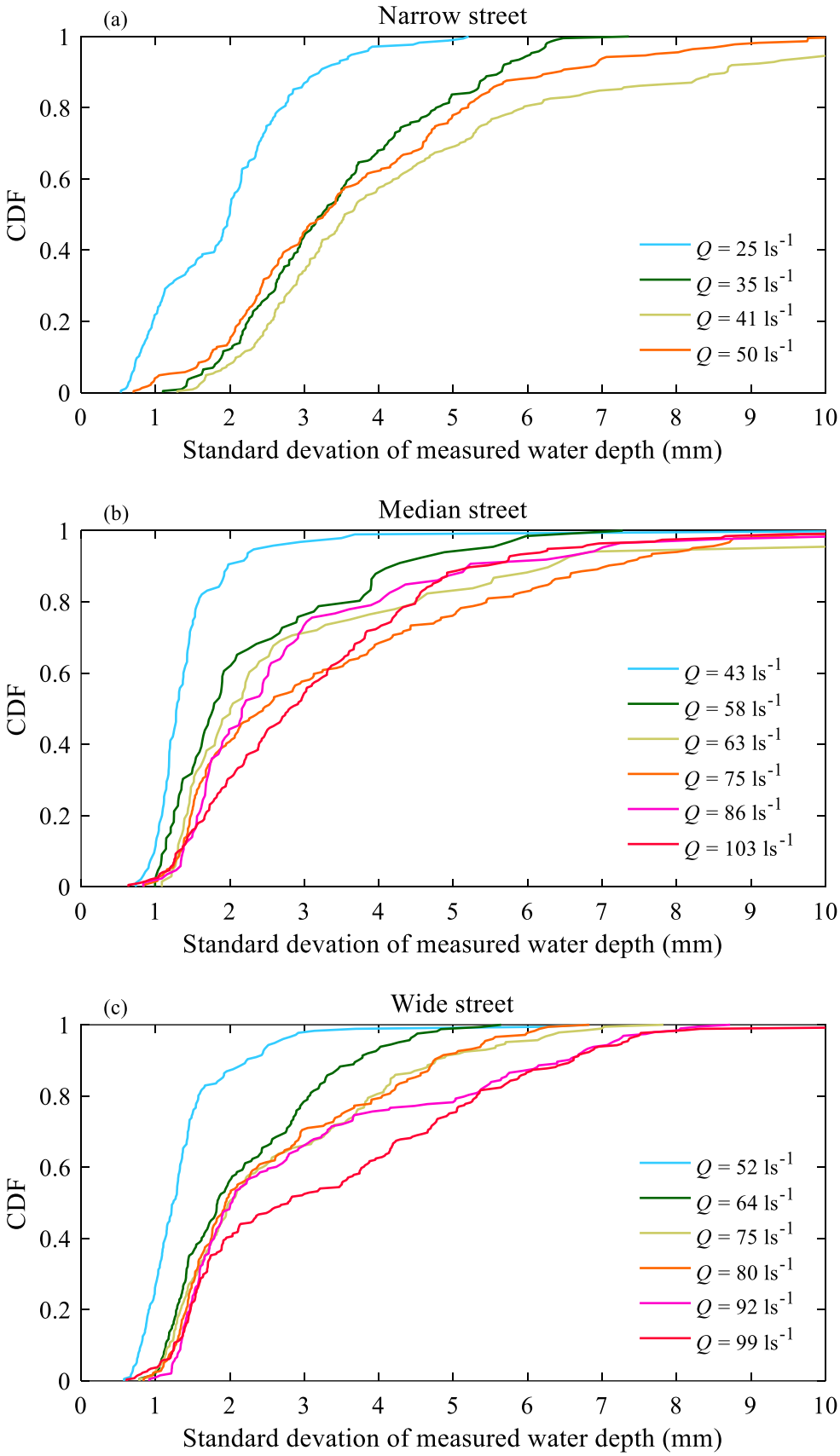

Figure S9: Cumulative distribution function (CDF) of the standard deviation water depth measurement of dataset by Velickovic et al. (2017)

Supplement 4: Profiles of measured water depths

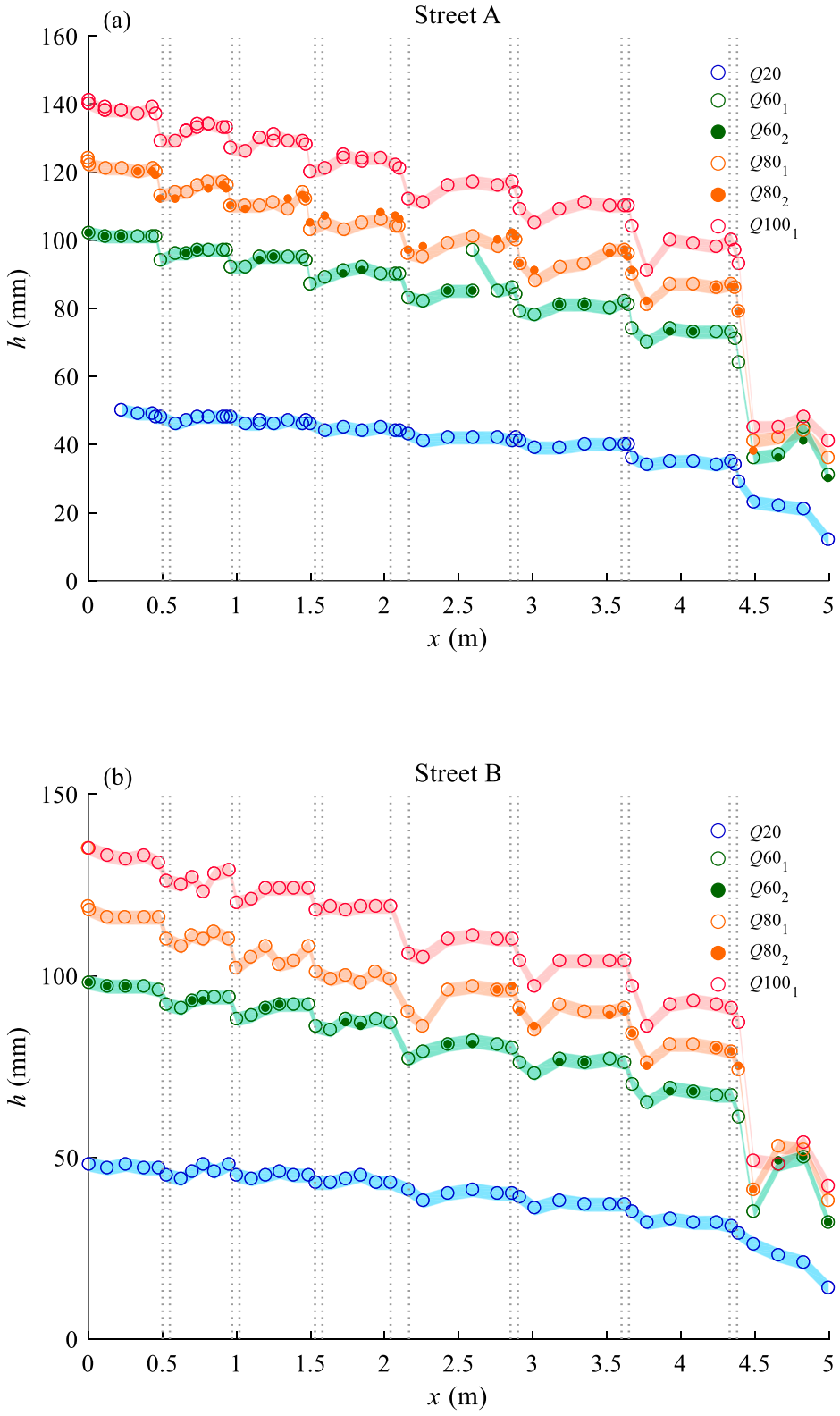

Figure S10: Measured water depth profiles in minor streets A and B in the dataset presented by Araud (2012). The colour shading represents 2 mm measurement uncertainty, subscripts 1 and 2 in legends represent the number of measurement repetitions, same for the following figures

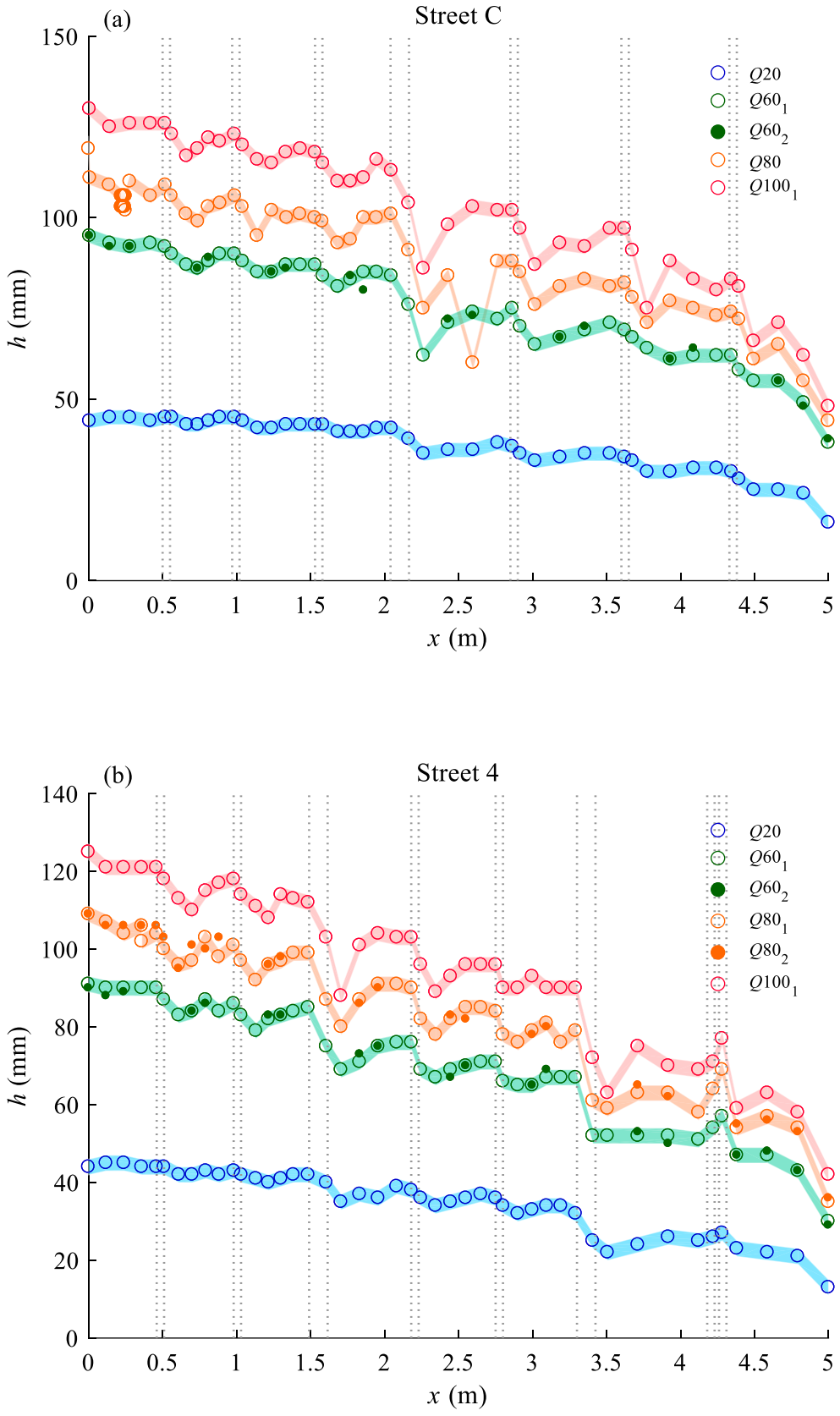

Figure S11: Measured water depth profiles in major streets C and 4 in the dataset of Araud (2012). The colour shading represents 2 mm measurement uncertainty

Supplement 5: Outflow discharge and uncertainty analysis

Several series of measurements of outflow discharges were conducted by Araud (2012) to assess the repeatability of the tests. Each series consisted in measurements performed over a duration of approximately 1 to 10 min. Figure S12, Figure S13, Figure S14 and Figure S15 provide boxplots of the measured flow partition (%) for each model run (Q_{in} = 20, 60, 80 and 100 m³/h) and each considered series of measurement repetition (labelled 1, 2 and 3). In the figure legends, N_1, N_2, and N_3 indicate the number of the measured repetitions. The median value of the flow partition remains very consistent from one measurements series to another. Therefore, the flow partition values kept for the analysis were derived by combining the various available time series.

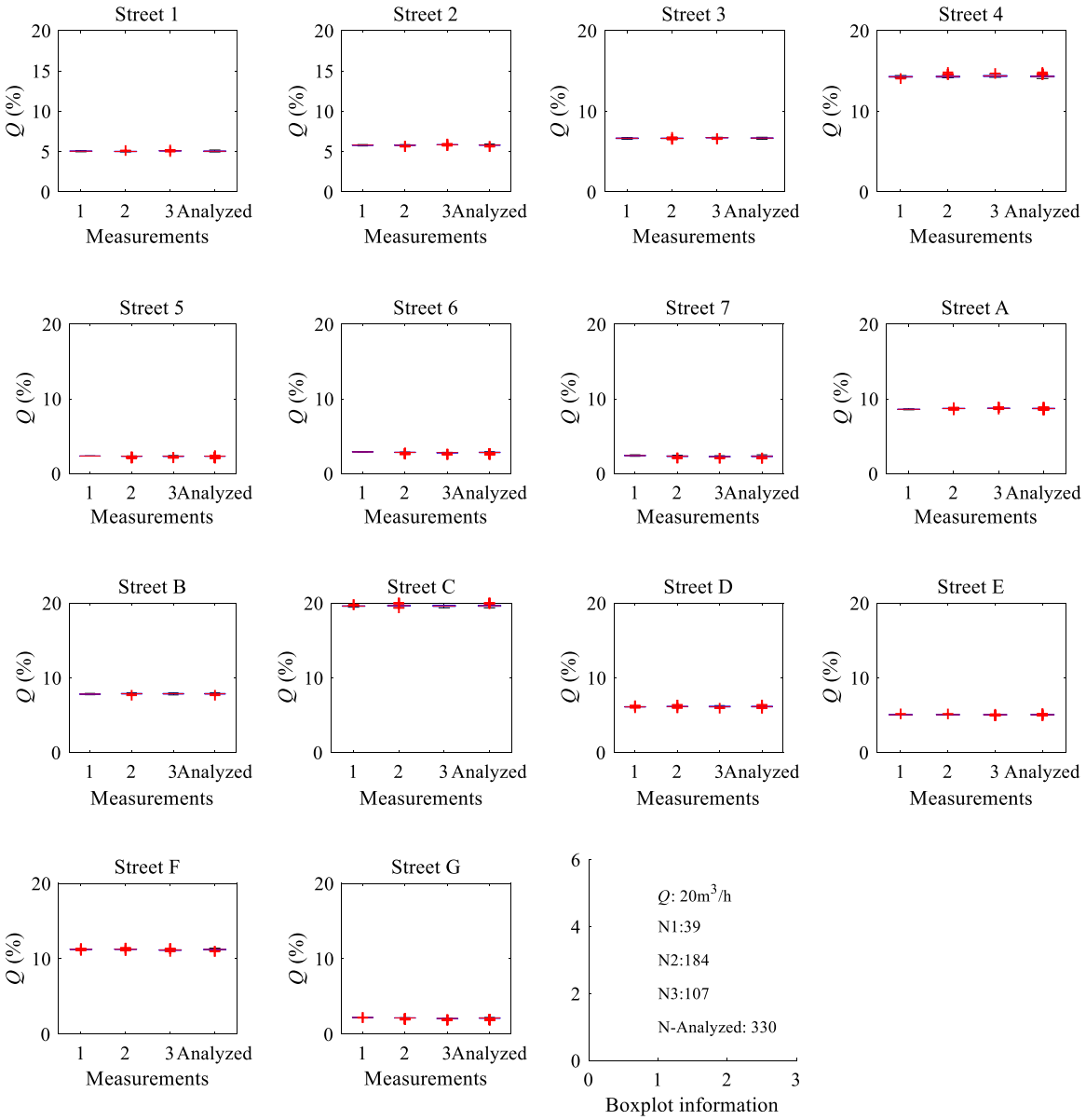

Figure S12: Boxplot of the measured outflow discharge partition in the experiments of Araud (2012) (Q_m = 20 m^3h^{-1})

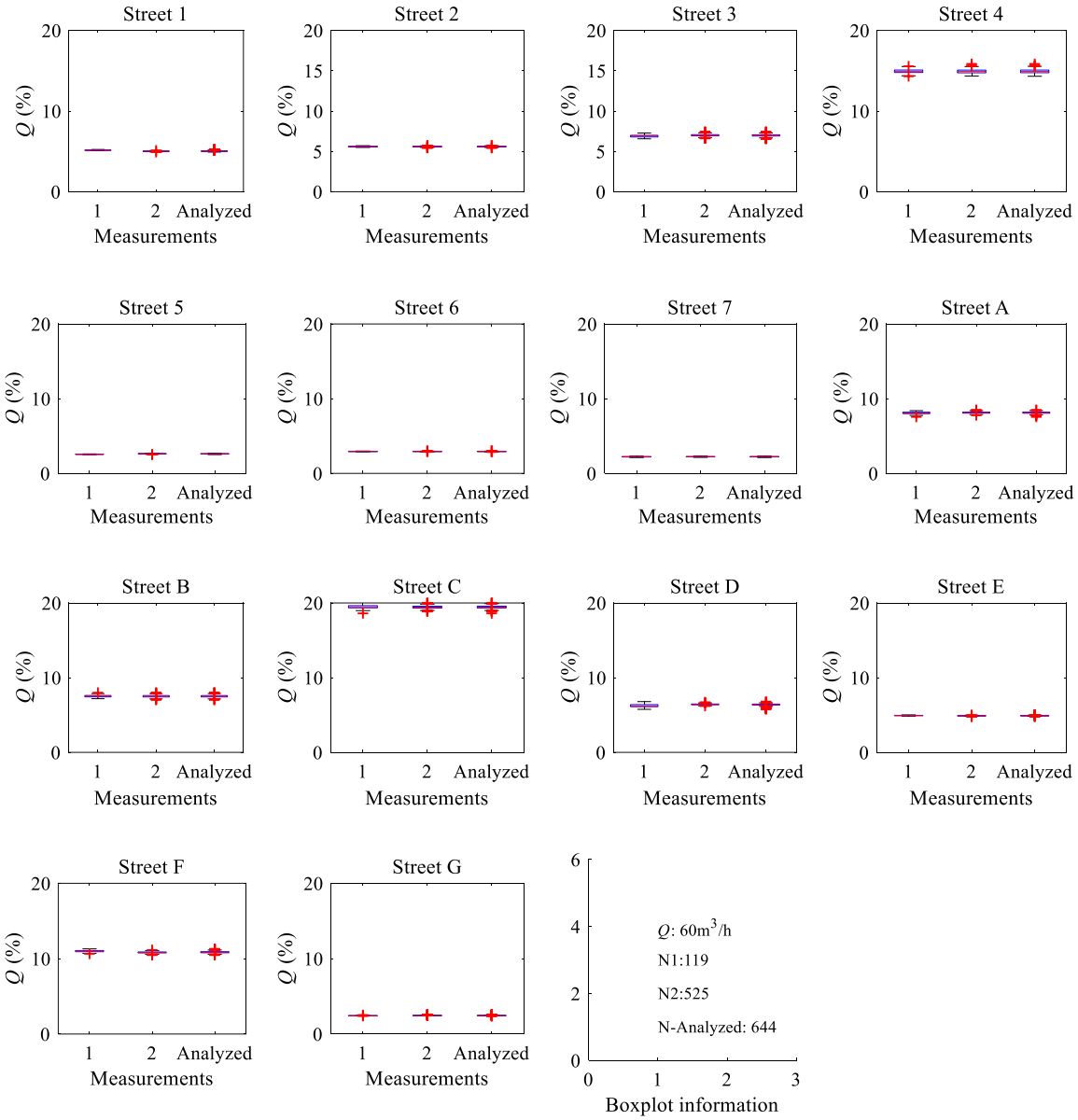

Figure S13: Boxplot of the measured outflow discharge partition in the experiments of Araud (2012) (Q_m = 60 m^3h^{-1})

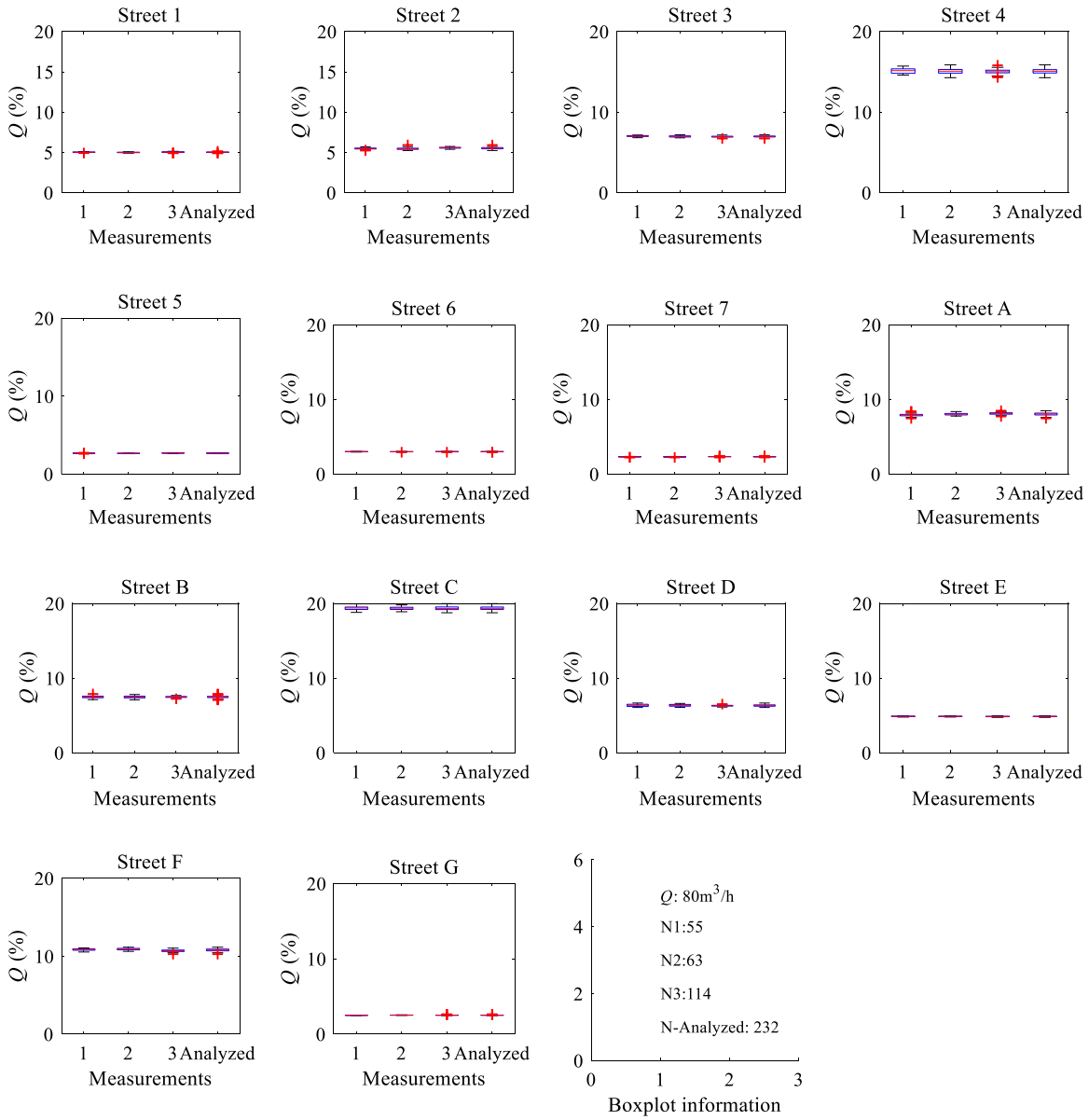

Figure S14: Boxplot of the measured outflow discharge partition in the experiments of Araud (2012) (Q_m = 80 m^3h^{-1})

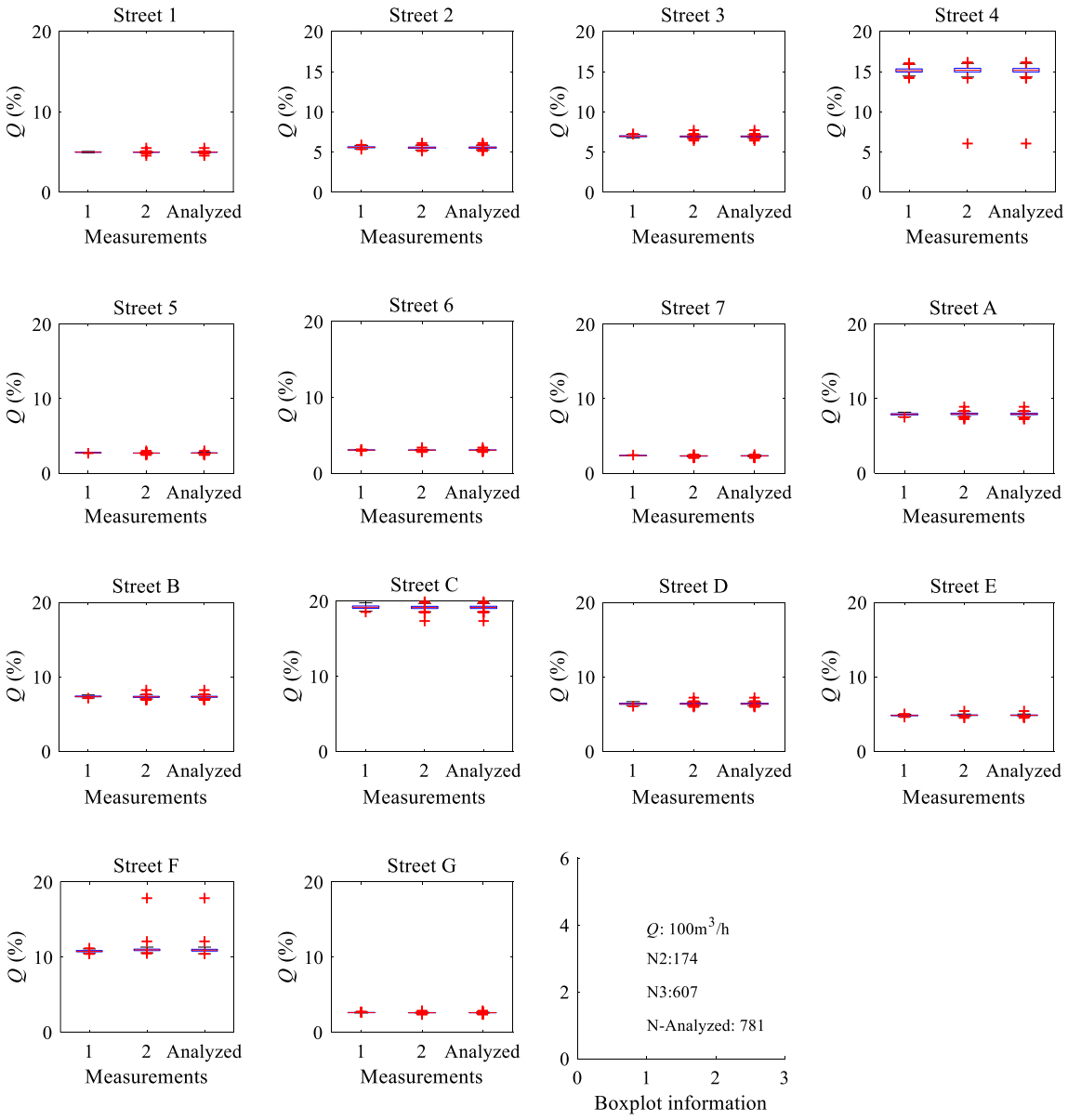

Figure S15: Boxplot of the measured outflow discharge partition in the experiments of Araud (2012) (Q_m = 100 m^3h^{-1})

The outflow discharge is estimated from a rating curve in Araud. (2012) as the equation following:

$$Q = 1333.3h^2$$

Where: Q is outflow discharge (m^3h^{-1}) and h is measured water depth (m). With the 1 mm measurement uncertainty, the measured flow discharge uncertainty is shown in Fig. S16 in function of corresponding flow charge.

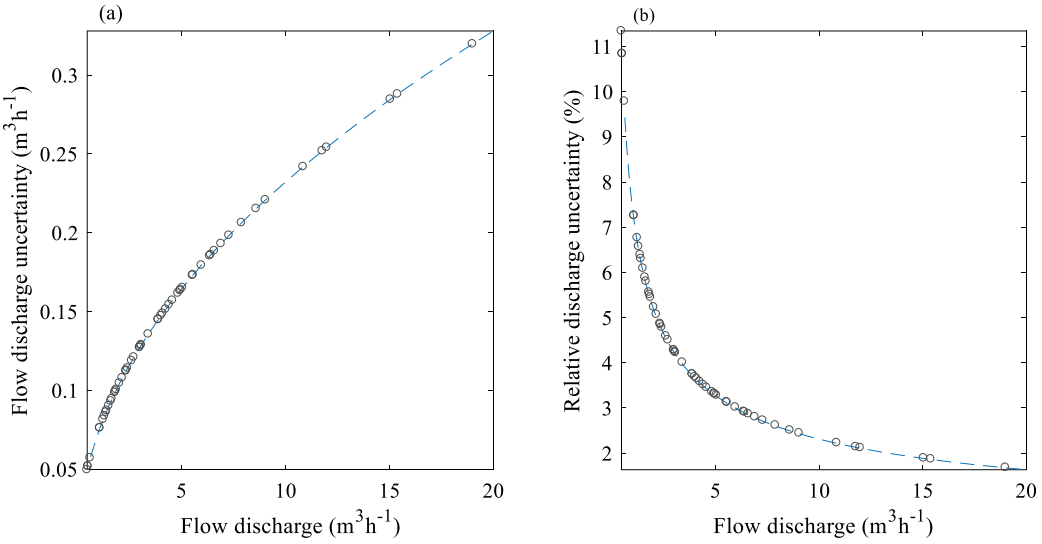

Figure S16: Measurement uncertainty analysis for the outflow discharge in the experiments of Araud (2012)

Supplement 6: Upscaled water depths based on the tests by Araud (2012)

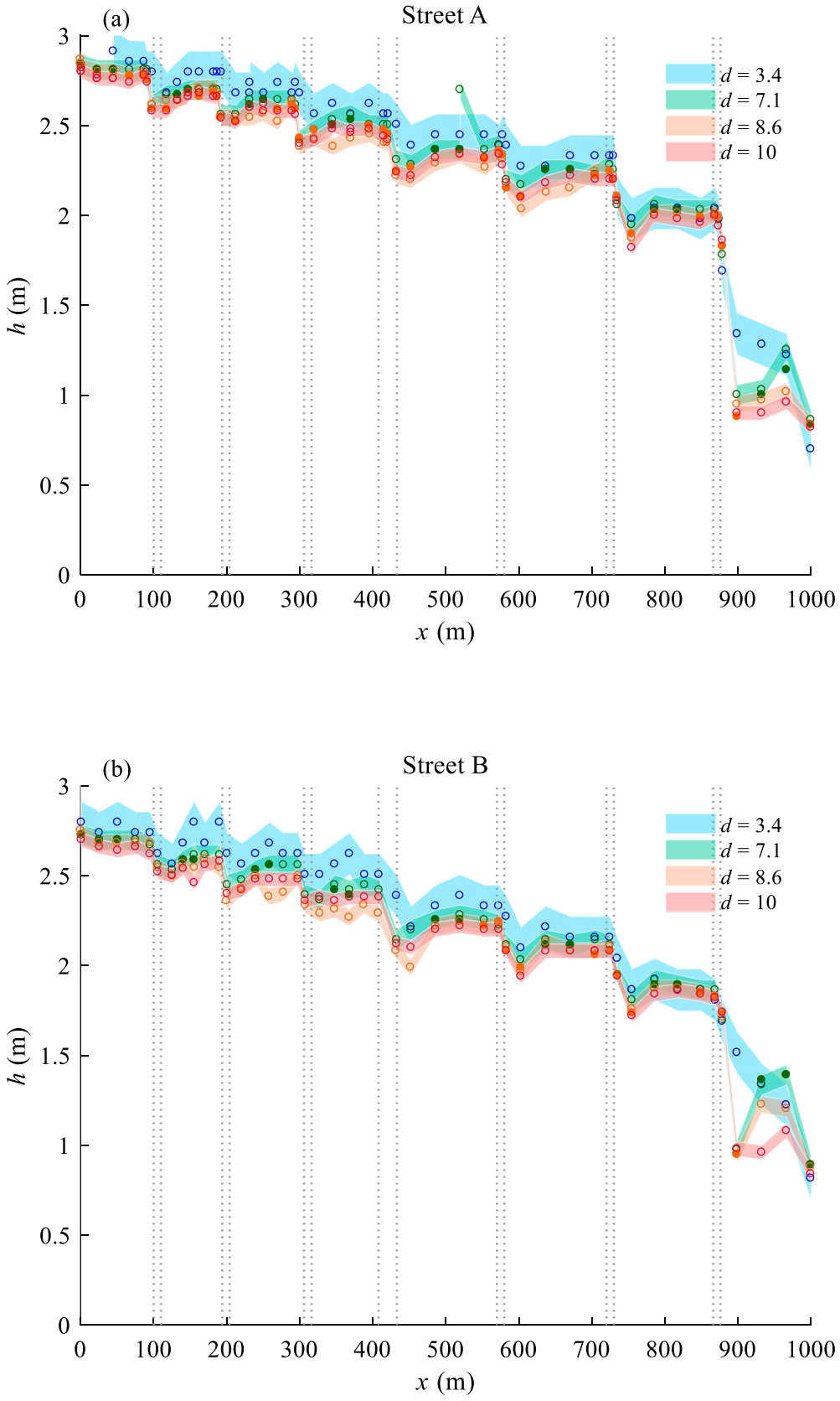

Figure S17: Upscaled water depth in prototype in minor streets A and B (dataset of Araud (2012))

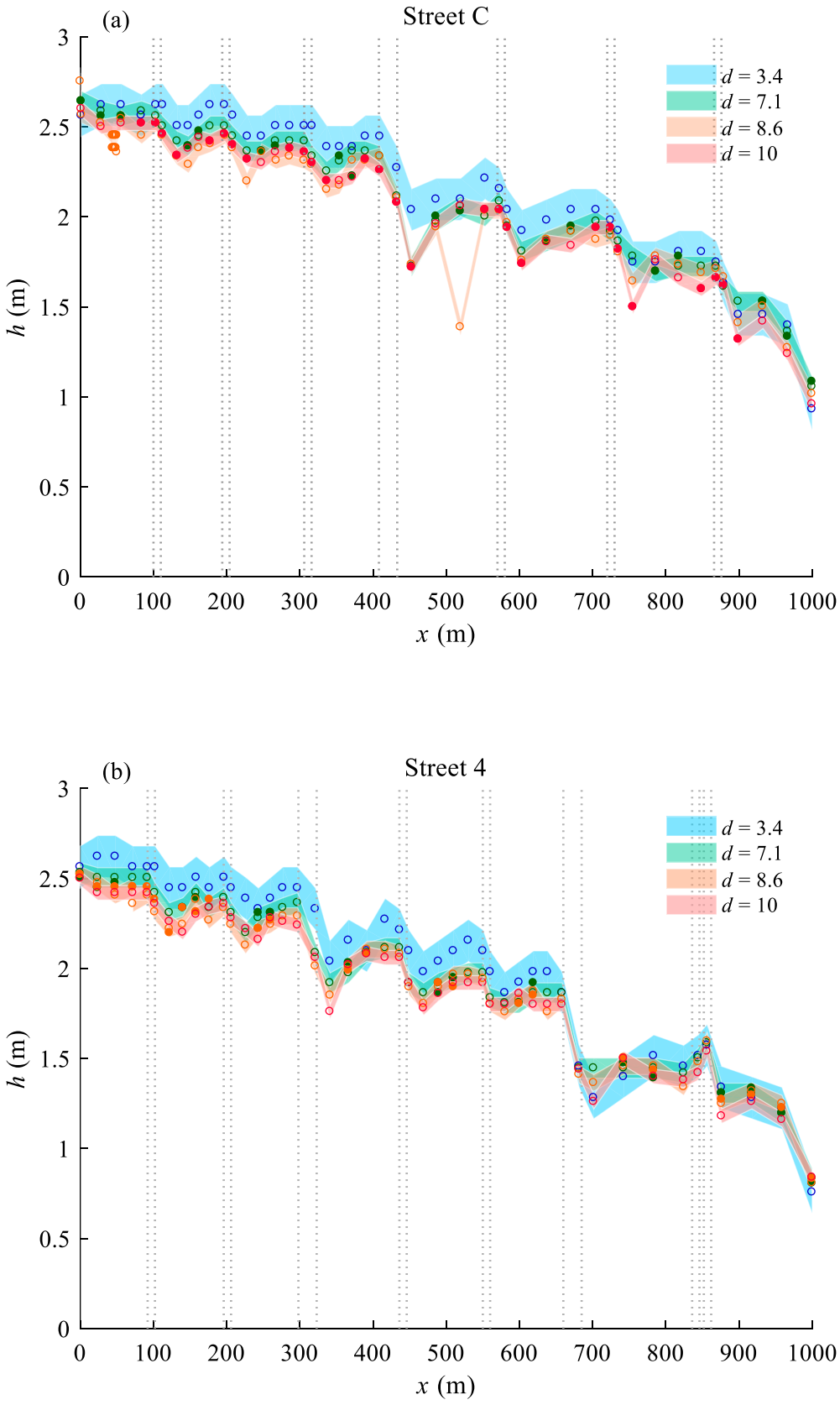

Figure S18: Upscaled water depth in prototype in major streets C and 4 (dataset of Araud (2012))

Supplement 7: Upscaled water depths based on the tests by Velickovic et al. (2017)

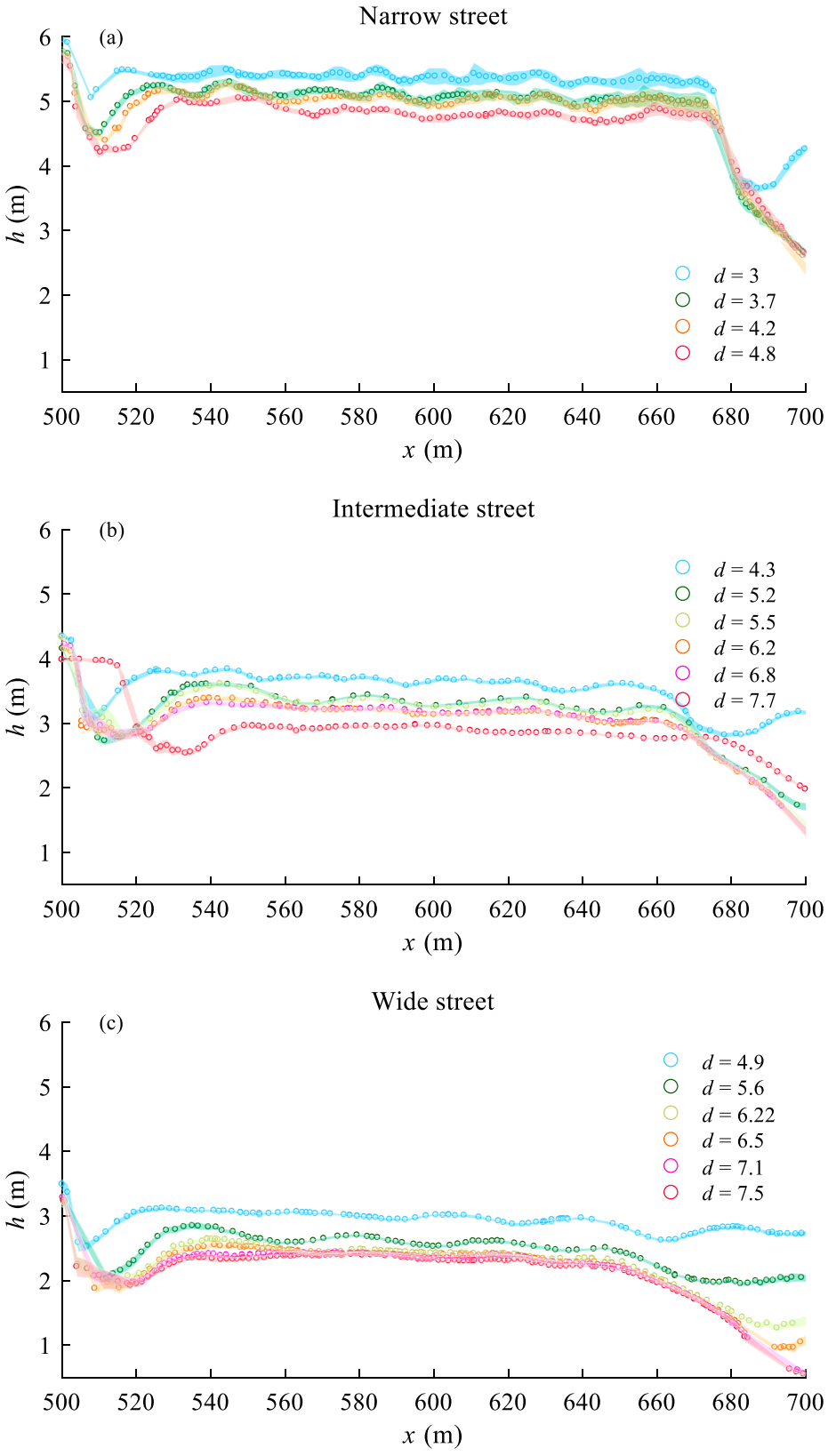

Figure S19: Upscaled water depth profiles, colour shade represents the corresponding upscaled measurement uncertainty (dataset by Velickovic et al. (2017)) in urban area

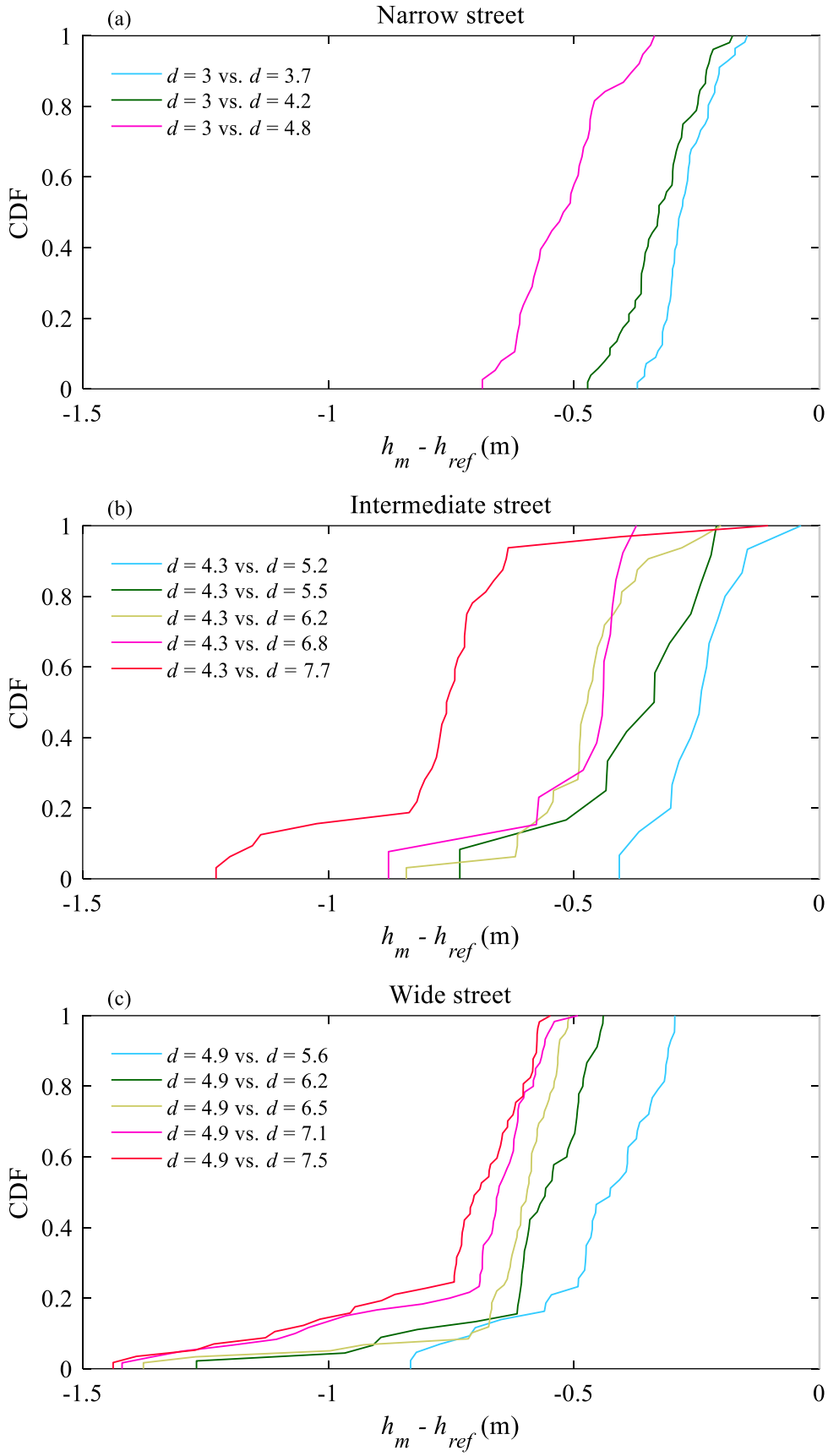

Figure S20: Cumulative distribution function (CDF) of the water depth difference between scale models and the reference model (dataset by Velickovic et al. (2017)) in urban area

Supplement 8: Upscaled outflow discharge based on the tests by Araud (2012) and Finaud-Guyot et al. (2018)

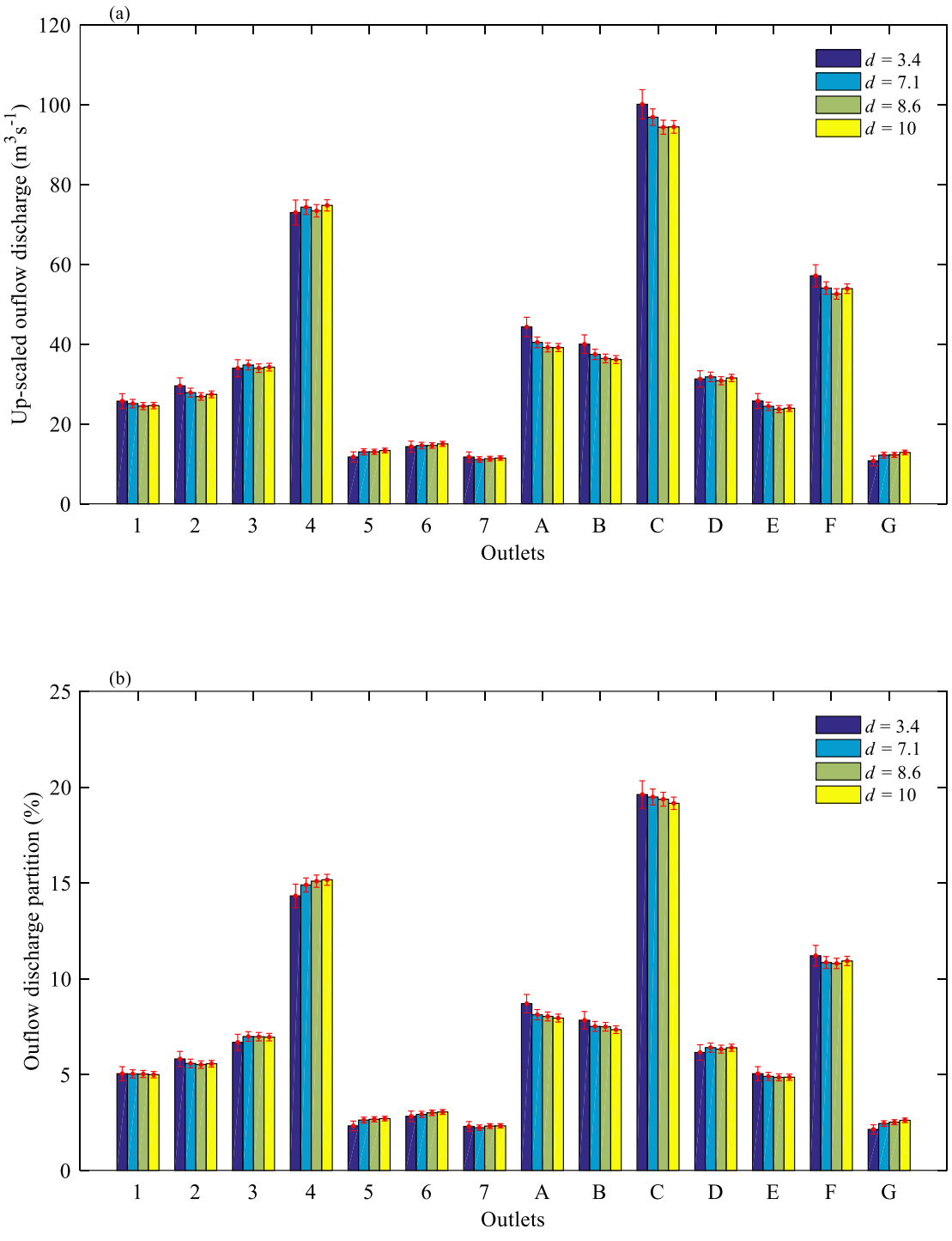

Figure S21: Outflow discharge at each street outlet: (a) as observed by Finaud-Guyot et al. (2018); (b) discharge partition in-between the streets (in % of the total).

Supplement 9: Change of water depth associated to a given change in outflow discharge

The Froude number F in the prototype may be estimated as follows:

$$\mathsf{F} = \frac{Q_p}{L_p\sqrt{gh_p^3}} = \frac{Q_m e_H e_V^{3/2}}{L_m e_H \sqrt{gh_p^3}} = \frac{Q_m e_V^{3/2}}{L_m\sqrt{gh_p^3}}$$

with Q_p, L_p and h_p representing, respectively, the discharge, street width and water depth at the prototype scale. Q_m and L_m are the discharge and the street width at the scale of a model characterized by horizontal and vertical scale factors equal to e_H and e_V, respectively.

Assuming that the upscaled flow conditions derived from various models (corresponding to different values $e_{V,i}$ of the vertical scale factor e_V) are nonetheless characterized by the same value of the Froude number, an "associated" water depth h_p may be estimated for each model (noted with subscript *i*), including the "reference" model (noted with subscript *ref*):

$$h_{p,i} = \left(\frac{Q_{m,i} e_{V,i}^{3/2}}{L_{m,i}\mathsf{F}\sqrt{g}}\right)^{2/3} \qquad \text{and} \qquad h_{p,ref} = \left(\frac{Q_{m,ref} e_{V,ref}^{3/2}}{L_{m,ref}\mathsf{F}\sqrt{g}}\right)^{2/3}$$

Finally, the ratio $h_{p,i} / h_{p,ref}$ may be calculated as:

$$\frac{h_{p,i}}{h_{p,ref}} = \left(\frac{\dfrac{Q_{m,i} e_{V,i}^{3/2}}{L_{m,i}\mathsf{F}\sqrt{g}}}{\dfrac{Q_{m,ref} e_{V,ref}^{3/2}}{L_{m,ref}\mathsf{F}\sqrt{g}}}\right)^{2/3} = \left(\frac{Q_{m,i} e_{V,i}^{3/2}}{Q_{m,ref} e_{V,ref}^{3/2}}\right)^{2/3} = \left(\frac{Q_{m,i}}{Q_{m,ref}}\right)^{2/3} \frac{e_{V,i}}{e_{V,ref}}$$

Supplement 10: Energy slope analytical analysis

$$S_{f,p} = \frac{e_V}{e_H} S_{f,m} = \frac{e_V}{e_H} \frac{f_m}{8} \frac{V_m^{\,2}}{gR_{H,m}} = \frac{1}{8} f_m \left(\mathrm{R}_m, \frac{k_{s,m}}{R_{H,m}} \right) \mathrm{F}^2 \frac{h_m}{R_{H,m}} \frac{e_V}{e_H}$$

Effect of viscosity

Effect of relative roughness height

Effect of aspect ratio

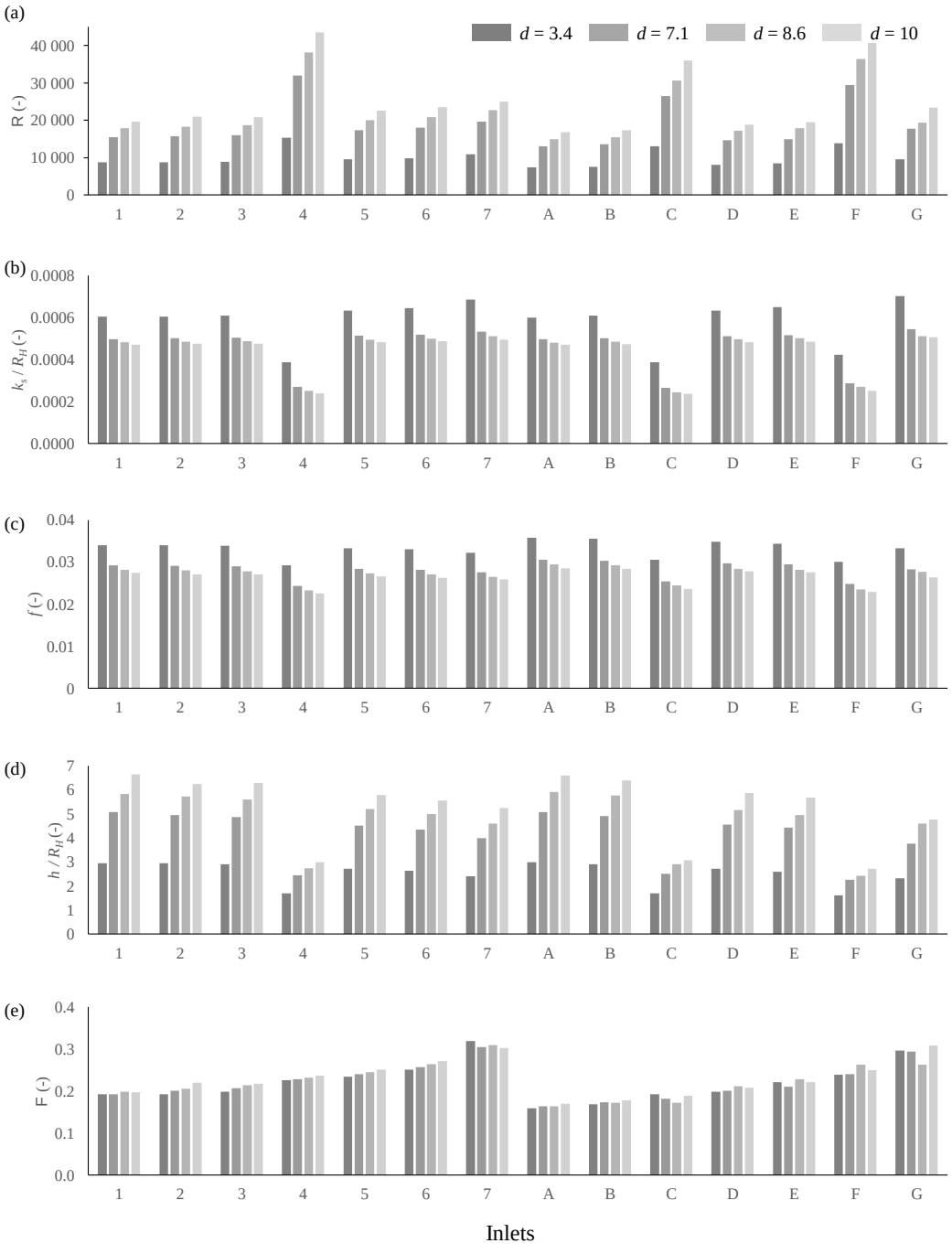

Figure S22: Effect of model distortion on the energy slope and influencing parameters for the experimental tests of Araud (2012).

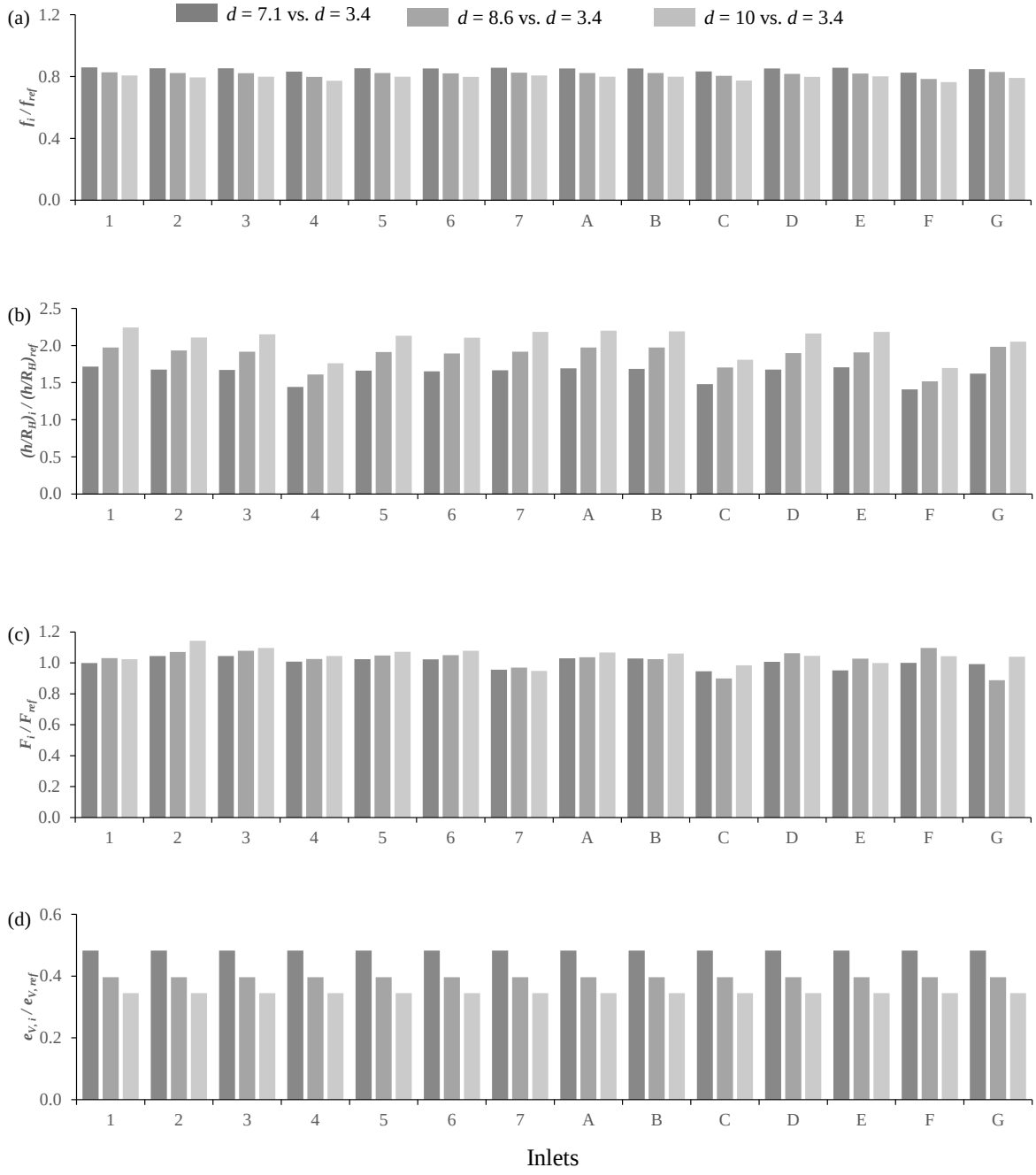

Figure S23: Relative value of the parameters involved in the estimation of the energy slope, compared to the same values in the reference model, i.e. with d = 3.4 (Run 4) (based on the dataset of Araud (2012)). Subscript i corresponds to a particular model run (d = 7.1, d = 8.6 or d = 10)